Supporting Information

Membrane lipid composition directs the cellular selectivity of antimicrobial metallohelices

Nicola J. Rogers,*[a,b] Miles L. Postings,[b] Ann M. Dixon,[b] John Moat,[c] Georgia Shreeve,[b] Louise Stuart,[b] Nick Waterfield,[d] Peter Scott.[b]

[a] Department of Chemistry, Hong Kong Baptist University, Kowloon Tong, Hong Kong
[b] Department of Chemistry, University of Warwick, Coventry CV4 7AL, UK
[c] School of Life Sciences, University of Warwick, Gibbet Hill Campus, Coventry, UK
[d] Warwick Medical School, University of Warwick, Coventry, UK

Contents

57Fe Compound characterisation data

Δ_{Fe}-[$^{57}Fe_2$(*R,R*-L^1)$_3$]Cl_4·6H_2O (Δ-**1'**)

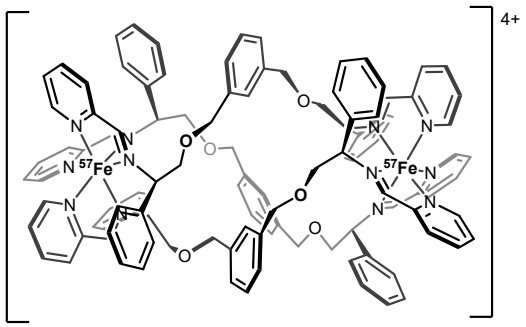

Δ_{Fe}-[$^{57}Fe_2$**L**$^1_3$]$^{4+}$

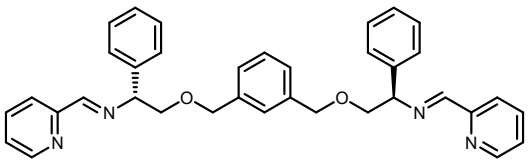

(*R,R*)-**L**^{1}

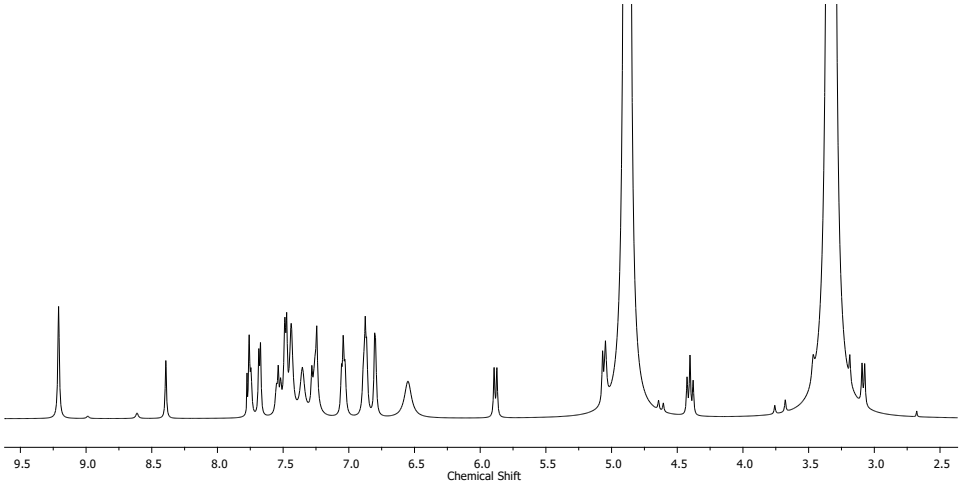

Figure S1. ^{1}H NMR (500 MHz, MeOD, 298 K) of Δ-**1**'.

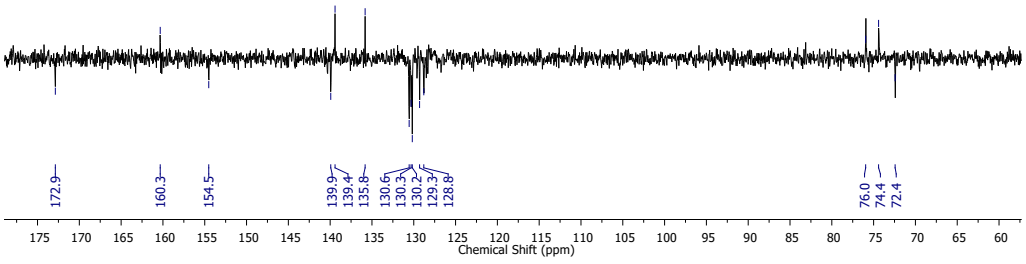

Figure S2. $^{13}C\{^1H\}$ APT NMR (126 MHz, MeOD, 298 K) of Δ-**1**'.

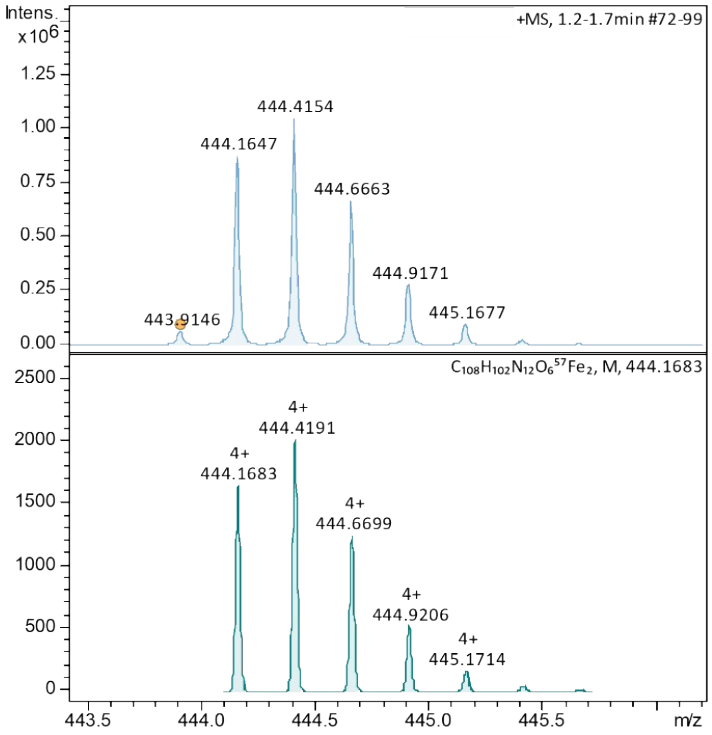

Figure S3. HRMS (+) of Δ-**1**', predicted (lower) and measured (upper) spectra.

Λ_{Fe}-[$^{57}Fe_2$(*S,S*-L^1)$_3$]Cl$_4$·6H$_2$O (Λ-**1'**)

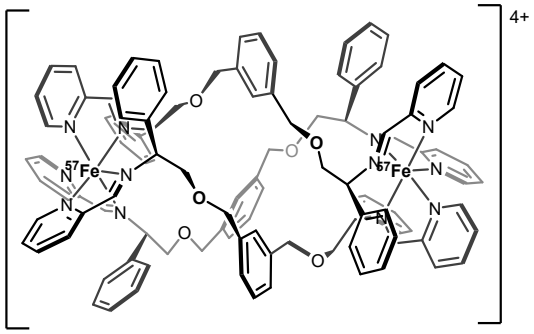

Λ_{Fe}-[$^{57}Fe_2$**L^1**$_3$]$^{4+}$

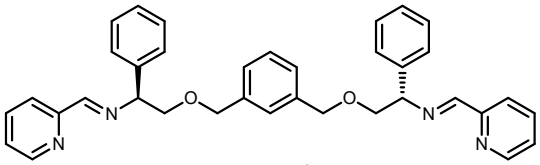

(*S,S*)-**L^1**

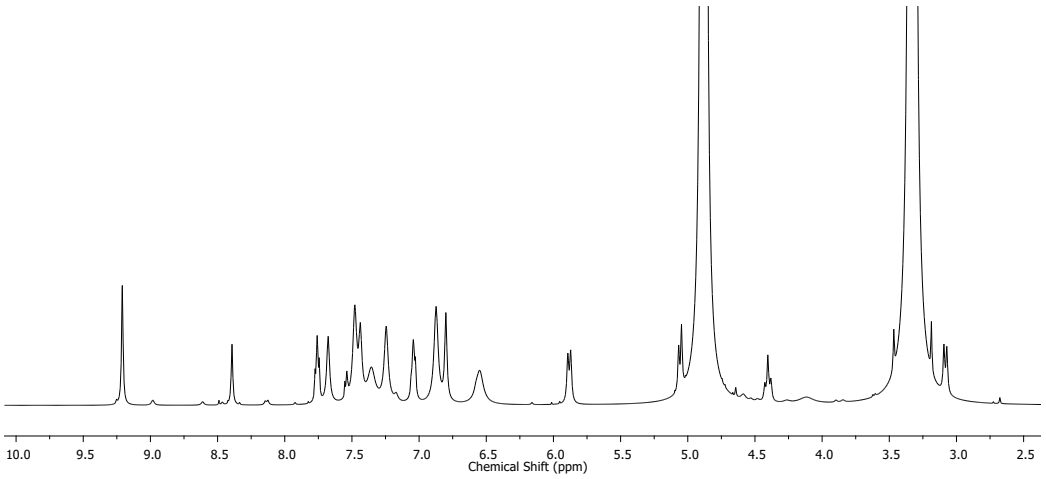

Figure S4. ^{1}H NMR (500 MHz, MeOD, 298 K) of Λ-**1**'.

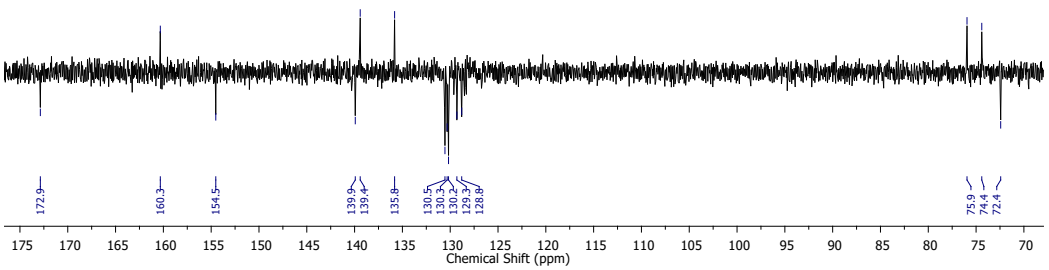

Figure S5. ^{13}C{^{1}H} APT NMR (126 MHz, MeOD, 298 K) of Λ-**1**'.

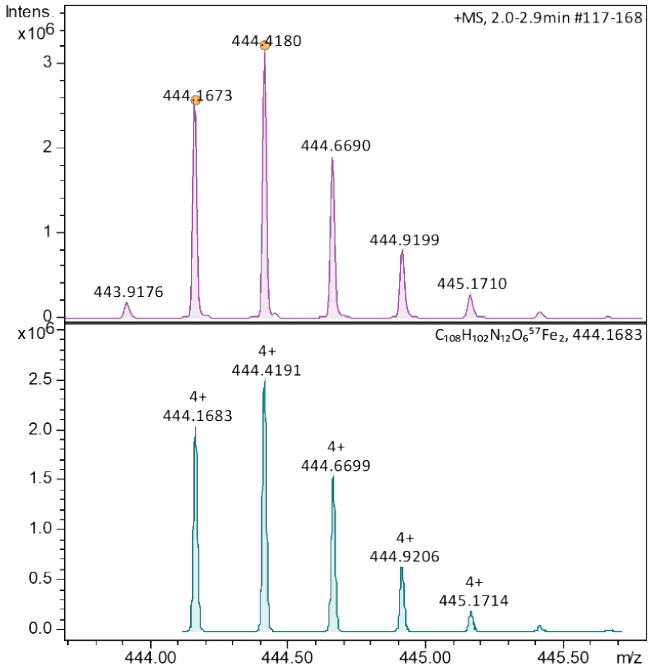

Figure S6. HRMS (+) of Λ-**1**', predicted (lower) and measured (upper) spectra.

Δ_{Fe}-[$^{57}Fe_2$(*R,R*-L^2)$_3$]Cl_4·6H_2O (Δ-**2'**)

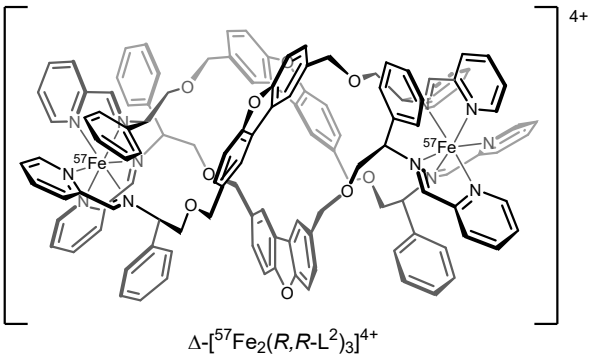

Δ-[$^{57}Fe_2$(*R,R*-L^2)$_3$]$^{4+}$

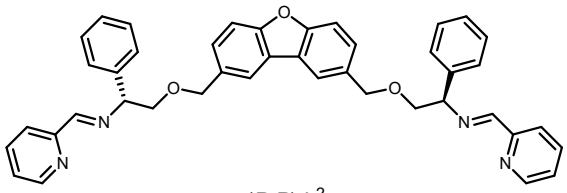

(*R,R*)-L^2

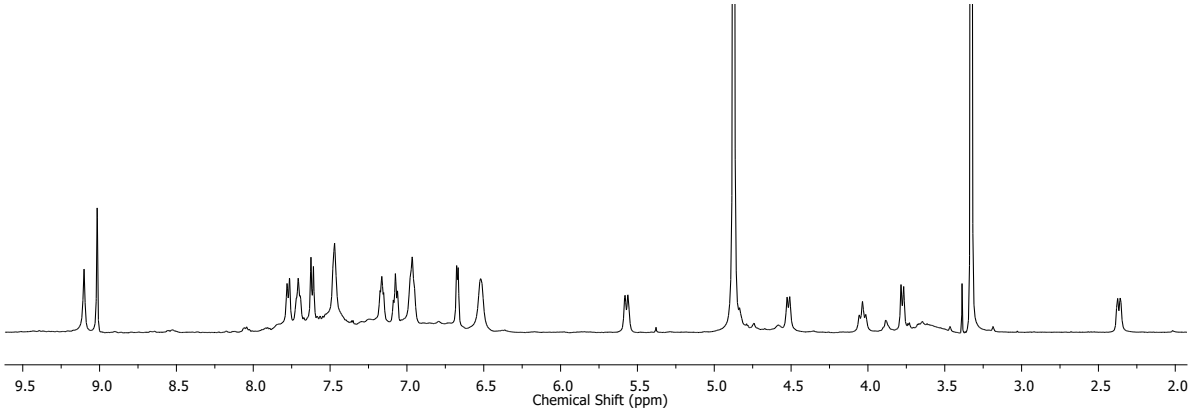

Figure S7. ^{1}H NMR (500 MHz, MeOD, 298 K) of Δ-**2**'.

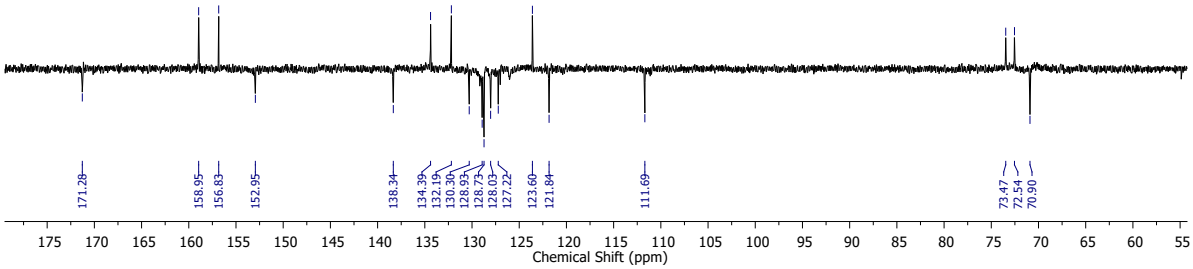

Figure S8. $^{13}C\{^1H\}$ APT NMR (126 MHz, MeOD, 298 K) of Δ-**2**'.

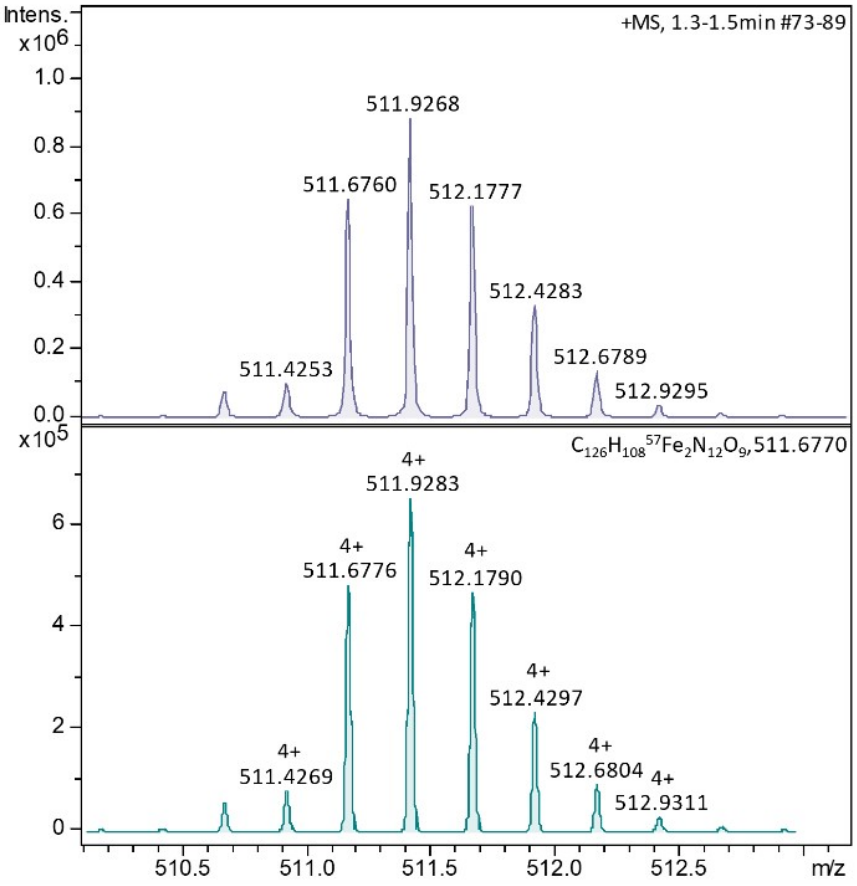

Figure S9. HRMS (+) of Δ-**2**', predicted (lower) and measured (upper) spectra.

Λ_{Fe}-[$^{57}Fe_2$(*S*,*S*-L^b)$_3$]Cl$_4$·6H$_2$O (**Λ-2'**)

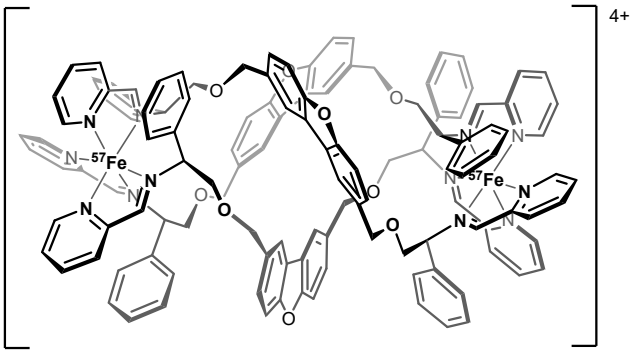

Λ-[$^{57}Fe_2$(*S*,*S*-L^2)$_3$]$^{4+}$

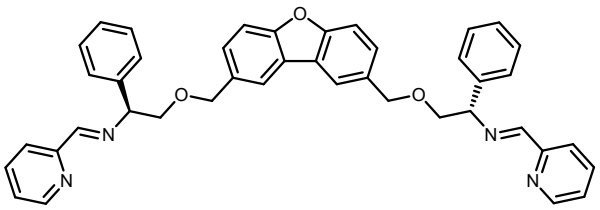

(*S*,*S*)-L^2

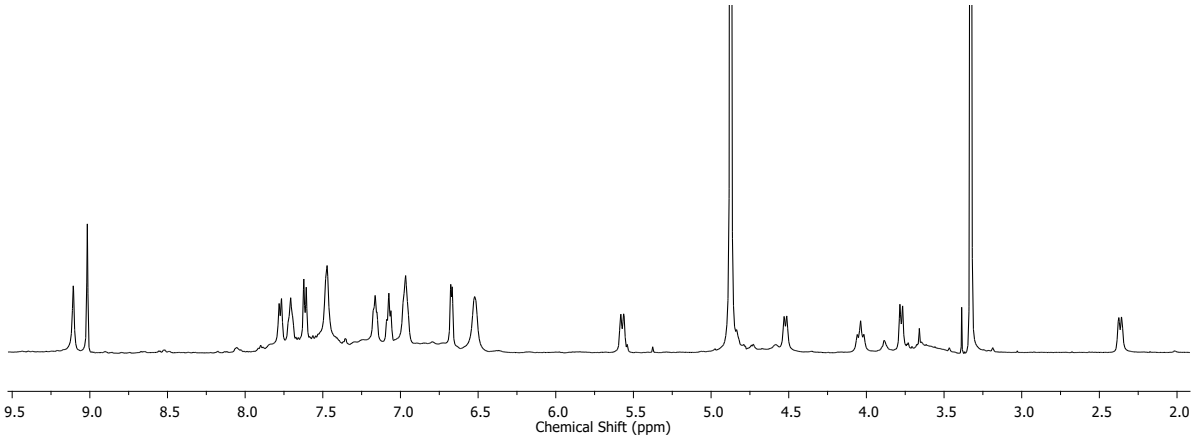

Figure S10. ^{1}H NMR (500 MHz, MeOD, 298 K) of Λ-**2'**.

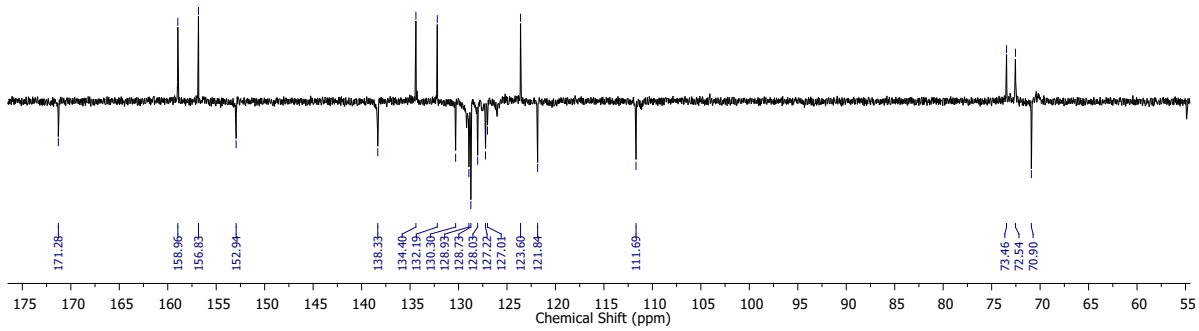

Figure S11. ^{13}C{^{1}H} APT NMR (126 MHz, MeOD, 298 K) of Λ-**2'**.

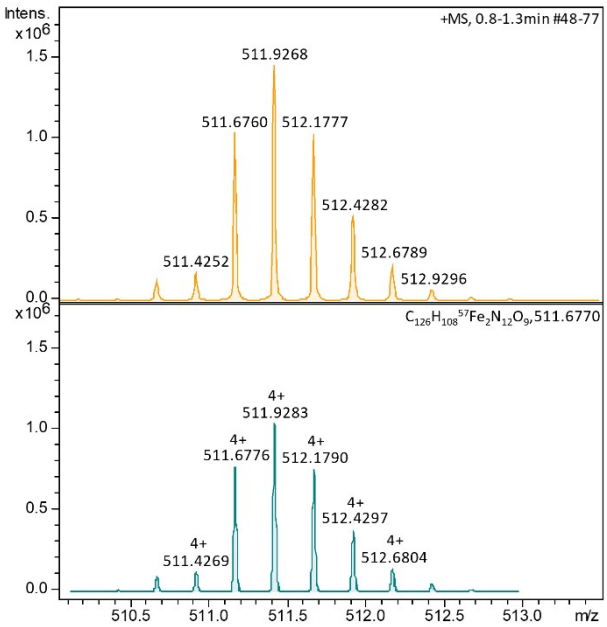

Figure S12. HRMS (+) of Λ-**2**', predicted (lower) and measured (upper) spectra.

Antimicrobial bactericidal data

Table S1. Minimum bactericidal concentrations against Gram-negative – E. coli and Gram-positive – S aureus bacteria, determined for Λ-**1**, Δ-**1**, Λ-**2**, and Δ-**2**.

	MBC/ μg mL^{-1} (μM)	
compound	*E. coli ATCC 25922*	*S. aureus 27853*
Λ-1	8 (3.9)	32 (15.7)
Δ-1	32 (15.7)	64 (31.3)
Λ-2	64 (26.4)	8 (3.3)
Λ-2	64 (26.4)	8 (3.3)

Antimicrobial activity and cellular accumulation studies of ^{57}Fe-metallohelices

Table S2. Iron (^{57}Fe) cellular accumulation (ng ^{57}Fe per 10^8 cells) in *S. aureus* USA300 bacteria when dosed with at 8 mg mL^{-1}, MIC, and 0.5×MIC concentrations for 20 h.

		Cellular accumulation of ^{57}Fe / ng per 10^8 cells		
Compound	MIC / μg mL^{-1}	dose = 8 μg mL^{-1}	dose = MIC	dose = 0.5MIC
Λ-**1'**	16	10.9±0.2	23.1±0.2	11.9±0.3
Δ-**1'**	16	10.0±0.2	19.0±0.3	9.55±0.23
Λ-**2'**	2	186±6	47.7±1.4	25.0±0.8
Δ-**2**	2	195±1	51.3±1.5	25.6±0.6

Table S3. Iron (^{57}Fe) cellular accumulation (ng ^{57}Fe per 10^8 cells) in *E. coli* TOP10 bacteria when dosed with at 8 mg mL^{-1}, MIC, and 0.5×MIC concentrations for 20 h.

		Cellular accumulation of ^{57}Fe / ng per 10^8 cells		
Compound	MIC / μg mL^{-1}	dose = 8 μg mL^{-1}	dose = MIC	dose = 0.5MIC
Λ-**1'**	2	138±4	36.0±2.2	18.3±0.2
Δ-**1'**	4	77.3±4.3	37.2±2.2	18.8±0.1
Λ-**2'**	16	90.4±21.9	319±18	163±4
Δ-**2'**	16	98.1±8.4	335±12	178±7

DLS Data – Effect of metallohelices on model vesicle size

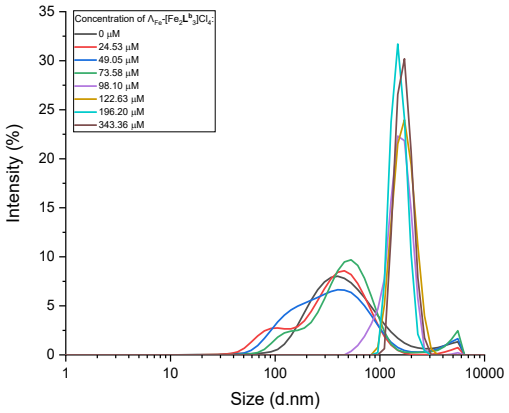

Figure S13 An overlay of the mean size (d/nm) distributions with regards to the scattering intensity (%) of *E. coli* cytosolic membrane-mimetic vesicles (~0.4 mM lipid) when 0 – 343 μM of Λ-**1** was added.

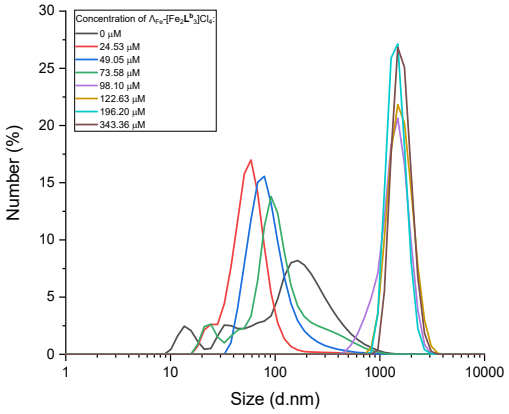

Figure S14 An overlay of the mean size (d/nm) distributions with regards to the calculated number distribution (%) of *E. coli* cytosolic membrane-mimetic vesicles (~0.4 mM lipid) when 0 – 343 μM of Λ-**1** was added.

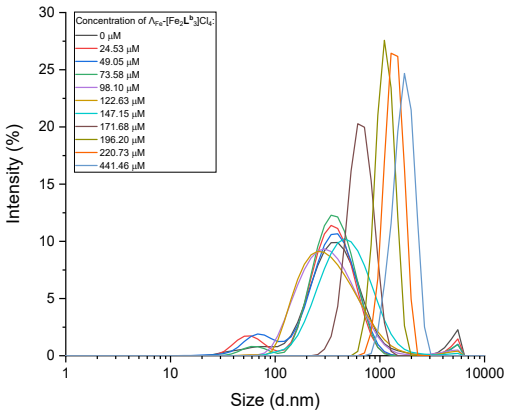

Figure S15 An overlay of the mean size (d/nm) distributions with regards to the scattering intensity (%) of *S. aureus* cytosolic membrane-mimetic vesicles (~0.4 mM lipid) when 0 – 441 μM of Λ-**1** was added.

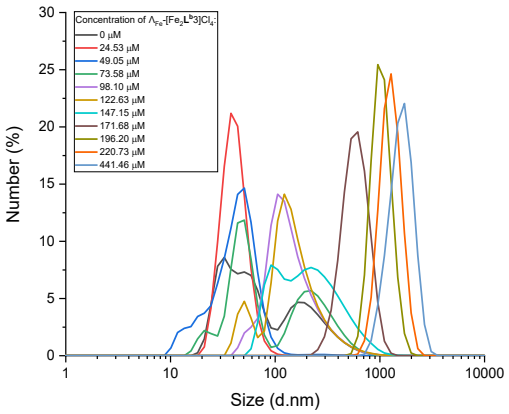

Figure S16 An overlay of the mean size (d/nm) distributions with regards to the calculated number intensity (%) of *S. aureus* cytosolic membrane-mimetic vesicles (~0.4 mM lipid) when 0 – 441 μM of Λ-**1** was added.

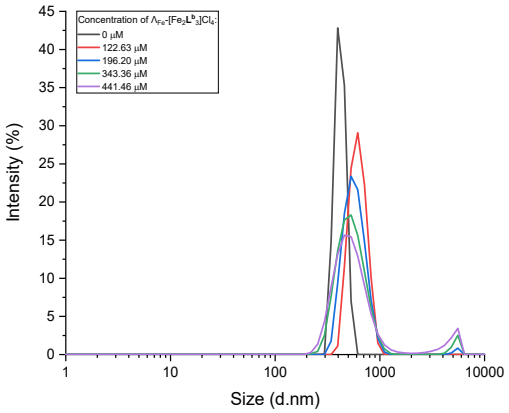

Figure S17 An overlay of the mean size (d/nm) distributions with regards to the scattering intensity (%) of mammalian plasma membrane-mimetic vesicles (~0.4 mM lipid) when 0 – 441 μM of Λ-**1** was added.

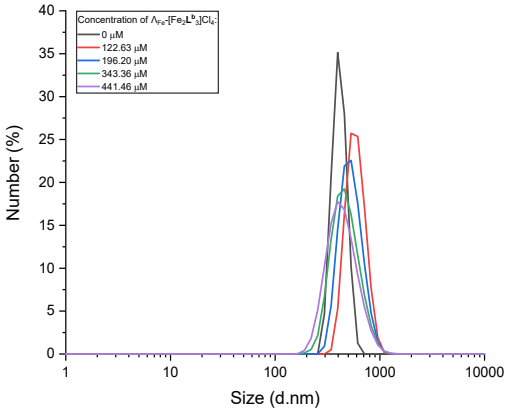

Figure S18 An overlay of the mean size (d/nm) distributions with regards to the calculated number distribution (%) of mammalian plasma membrane-mimetic vesicles (~0.4 mM lipid) when 0 – 441 μM of Λ-**1** was added.

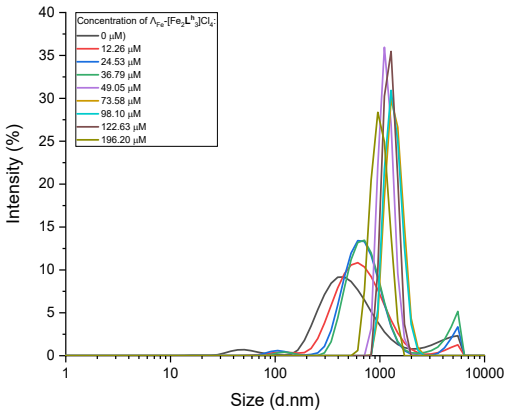

Figure S19 An overlay of the mean size (d/nm) distributions with regards to the scattering intensity (%) of *E. coli* cytosolic membrane-mimetic vesicles (~0.4 mM lipid) when 0 – 196 μM of Λ-**2** was added.

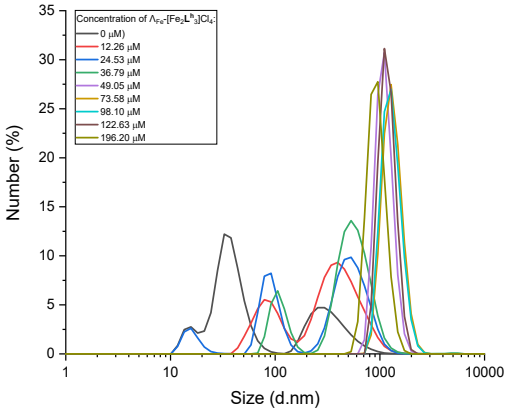

Figure S20 An overlay of the mean size (d/nm) distributions with regards to the calculated number distribution (%) of *E. coli* cytosolic membrane-mimetic vesicles (~0.4 mM lipid) when 0 – 196 μM of Λ-**2** was added.

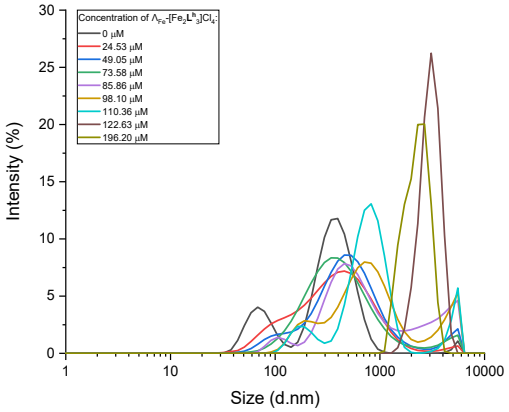

Figure S21 An overlay of the mean size (d/nm) distributions with regards to the scattering intensity (%) of *S. aureus* cytosolic membrane-mimetic vesicles (~0.4 mM lipid) when 0 – 196 μM of Λ-**2** was added.

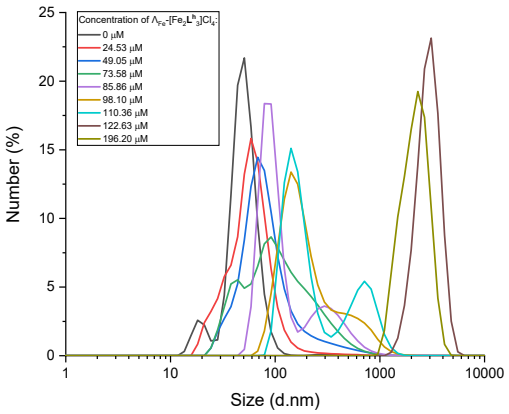

Figure S22 An overlay of the mean size (d/nm) distributions with regards to the calculated number distribution (%) of *S. aureus* cytosolic membrane-mimetic vesicles (~0.4 mM lipid) when 0 – 196 μM of Λ-**2** was added.

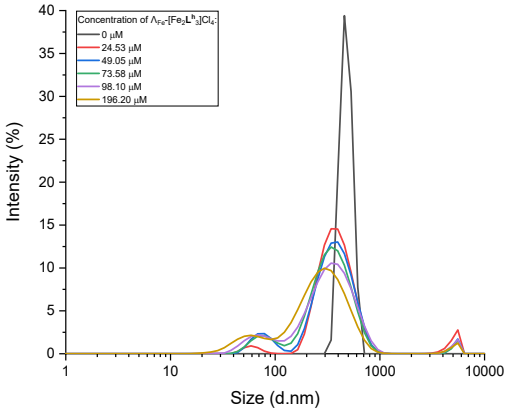

Figure S23 An overlay of the mean size (d/nm) distributions with regards to the scattering intensity (%) of mammalian plasma membrane-mimetic vesicles (~0.4 mM lipid) when 0 – 196 μM of Λ-**2** was added.

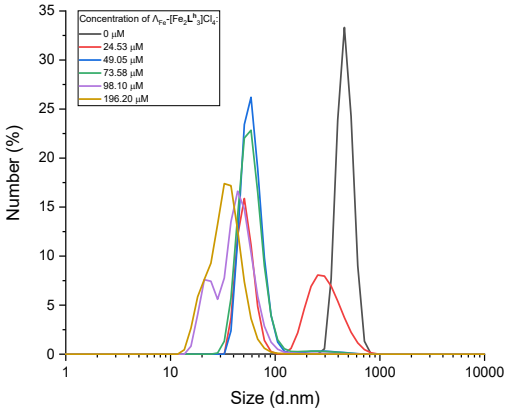

Figure S24 An overlay of the mean size (d/nm) distributions with regards to the calculated number distribution (%) of mammalian plasma membrane-mimetic vesicles (~0.4 mM lipid) when 0 – 196 μM of Λ-**2** was added.

*DLS data– Comparing the effects of enantiomers of **1***

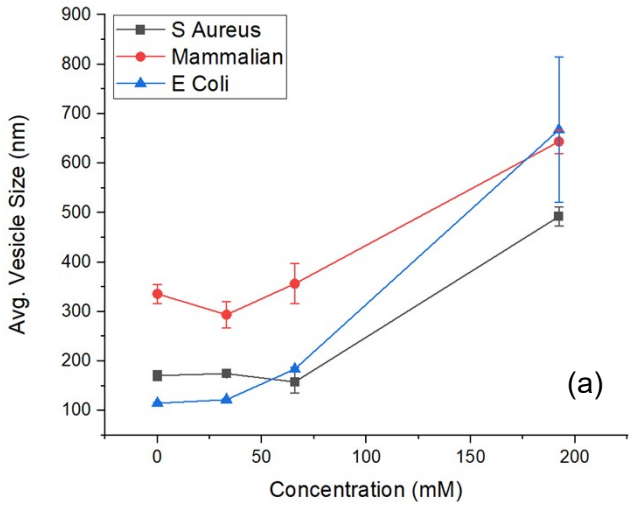

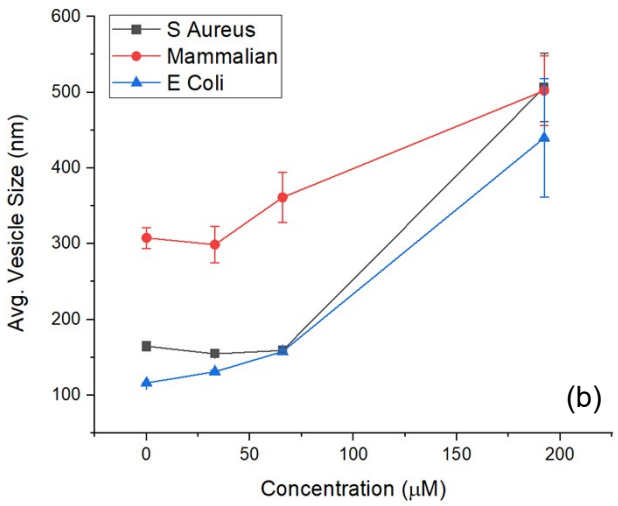

Figure S25 The mean Z-average size of membrane-mimetic vesicles (~0.6 mM lipid) when 0 – 192 μM of Λ-**1** (a) or Δ-**1** (b) was added.

Similar effects on the vesicle size data was observed upon titration of Λ-**1** and Δ-**1.**

Zeta Potential Data – Effect of metallohelices on model vesicle surface charge

Table S4. *Bacteria model vesicles.* Zeta potential measurements of 0.5 mg mL^{-1} unilamellar vesicles ([lipid] ~ 0.6 mM) plus 0-192 mM metallohelix in sodium phosphate buffer (25 mM, pH 7.4).

	Zeta Potential / mV					
	E. coli mimetic unilamellar vesicles			*S. aureus mimetic unilamellar vesicles*		
[MH] / μM	Λ-1	Δ-1	Λ-2	Λ-1	Δ-1	Λ-2
0	-50.2±1.3	-52.3±1.9	-48.5±1.0	-64.1±1.2	-64.1±0.4	-62.8±0.4
33	-25.1±1.1	-26.8±1.2	-28.0±0.6	-52.4±2.8	-53.9±3.2	-50.8±2.1
66	-19.8±0.4	-17.0±0.4	-8.4±3.5	-46.4±2.0	-41.5±1.2	-47.3±1.4
192	-10.8±0.2	-12.9±0.3	-8.3±0.3	-27.6±3.9	-21.2±0.5	+6.9±0.3

Table S5. *Mammalian model vesicles.* Zeta potential measurements of 0.5 mg mL^{-1} unilamellar vesicles ([lipid] ~ 0.6 mM) plus 0-192 mM metallohelix in sodium phosphate buffer (25 mM, pH 7.4).

	Zeta Potential / mV		
	Mammalian mimetic unilamellar vesicles		
[MH] / μM	Λ-1	Δ-1	Λ-2
0	-5.7±0.1	-8.1±0.4	-5.5±0.3
33	-4.7±0.3	-6.2±0.7	+14.7±0.4
66	-1.5±0.1	-5.0±0.4	+18.3±0.8
192	+4.6±0.5	+2.0±0.9	+21.3±0.7

Fitting Zeta potential data – Binding constants

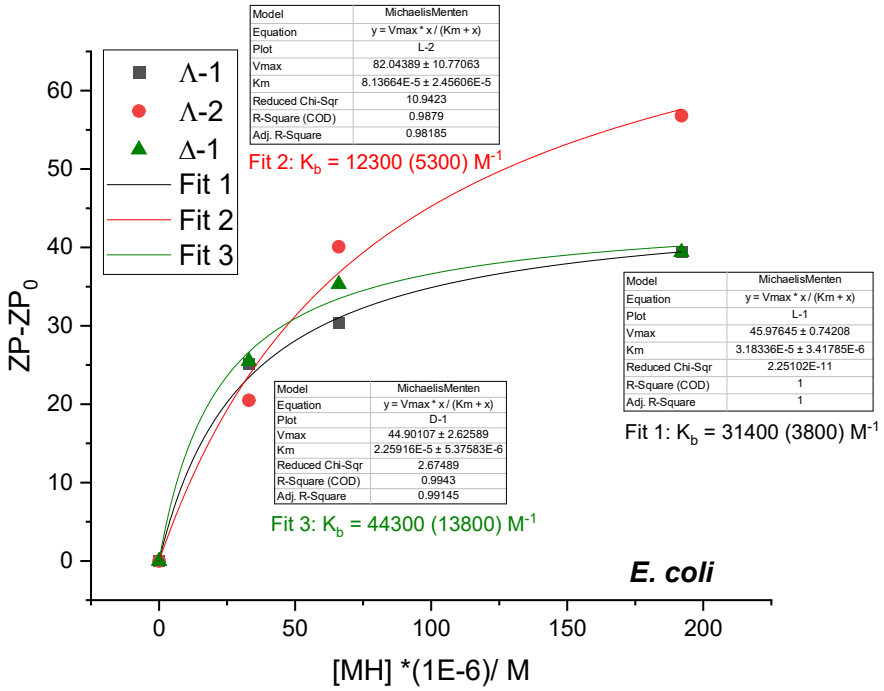

Figure S26 Fitting Zeta potential data. Zeta potential measurements of 0.5 mg mL^{-1} unilamellar *E. coli* vesicles ([lipid] ~ 0.6 mM), following the addition of 0-192 mM Λ-**1**, Λ-**2**, and Δ-**1**, in sodium phosphate buffer (25 mM, pH 7.4).

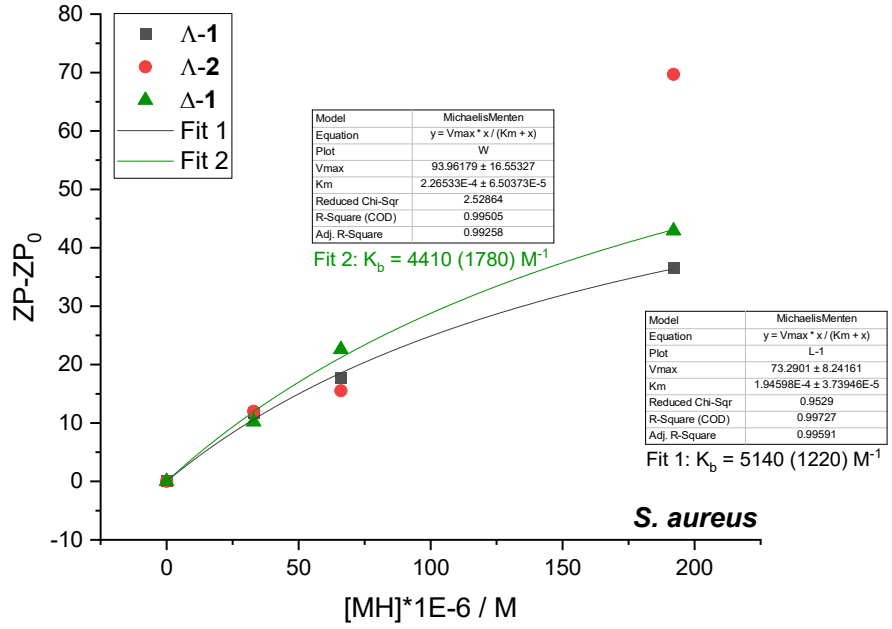

Figure S27 Fitting Zeta potential data. Zeta potential measurements of 0.5 mg mL^{-1} unilamellar *S. aureus* vesicles ([lipid] ~ 0.6 mM), following the addition of 0-192 mM Λ-**1** and Δ-**1**, in sodium phosphate buffer (25 mM, pH 7.4). It was not possible to fit the data following addition of Λ-**2**.

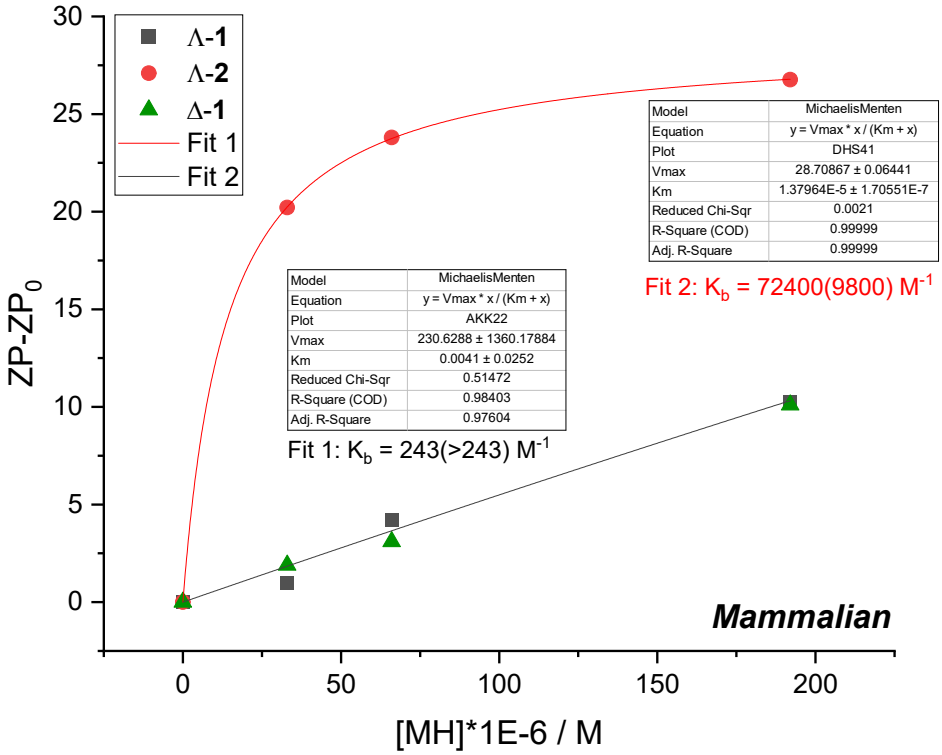

Figure S28 Fitting Zeta potential data. Zeta potential measurements of 0.5 mg mL^{-1} unilamellar mammalian vesicles ([lipid] ~ 0.6 mM), following the addition of 0-192 mM Λ-**1**, Λ-**2**, and Δ-**1**, in sodium phosphate buffer (25 mM, pH 7.4).

Table S6. Apparent Binding constants (K_{app}) of metallohelices with model membranes, estimated from zeta potential titrations

	E. coli	*S. aureus*	*Mammalian*
Λ-**1**	$3.1\pm0.4\times10^4$	$5.1\pm1.2\times10^3$	-[a]
Δ-**1**	$4.4\pm1.4\times10^4$	$4.4\pm1.8\times10^3$	-[a]
Λ-**2**	$1.2\pm0.5\times10^4$	-[b]	$7.2\pm1.0\times10^4$

[a] Cannot fit data due to negligible changes in zeta potential
[b] Cannot fit data – looks like two binding events